Application of Multiple Grids Topology to Supersonic Internal/External Flow Interactions

M. Kathong*
Old Dominion University, Norfolk, Virginia
R. E. Smith†
NASA Langley Research Center, Hampton, Virginia
and
S. N. Tiwari‡
Old Dominion University, Norfolk, Virginia

A multiblock grid with conservative interfacing is applied to compute supersonic Euler flow about and through a fighter airplane configuration. An efficient procedure called the "Ramshaw technique" is applied to conservatively transfer fluxes across discontinuous grid interfaces. The approach is called multiple grid and the numerical solution scheme is the finite-volume technique. Steady-state solutions are presented for Mach 2 at 0-, 3.79-, 7-, and 10-deg angles of attack. The results demonstrate that the multiple grid approach with conservative interfacing is capable of computing the flows about complex configurations. They further demonstrate the feasibility of generating independent grid blocks that can be patched together for flow computations.

Nomenclature

A_{ij}	= surface area of an arbitrary grid cell
A_p	= area of polygon
E	= total energy, $= \rho e + 0.5(u^2 + v^2 + w^2)$
e	= internal energy
F	= fluxes (mass, momentum, energy) in x direction
G	= fluxes in y direction
H	= fluxes in z direction
h_{ij}	= fluxes per unit area, $= H_{ij}/A_{ij}$
n_x, n_y, n_z	= surface normal in x, y, z directions
P	= pressure
q	= state variables, $= q_{i,j,k}$ at the cell center
u, v, w	= x, y, z components of velocity
VOL	= volume of a particular grid cell, $= \mathrm{VOL}_{i,j,k}$
x, y, z	= spatial coordinate
γ	= specific heat ratio
$\partial\Omega$	= boundary of an arbitrary domain
ρ	= density
Ω	= an arbitrary domain

Introduction

SIGNIFICANT improvements in numerical methods and computer technology in recent years have made it possible to solve inviscid compressible flow about moderately complex geometries using the Euler equations.[1,2] An important aspect of the flowfield computation is the generation of grids. Accurate solutions to the governing equations depend on the characteristics of the underlying grid, i.e., a grid that maps into a single computational box. This type of grid is very desirable due to its simplicity. However, for very complex geometries, such as complete airplane configuration, it is very difficult to construct single-block grids with desired properties, i.e., smoothness, orthogonality, and concentrations in appropriate locations. An alternate approach is to use several grid blocks, each possibly in a different coordinate system. This approach,

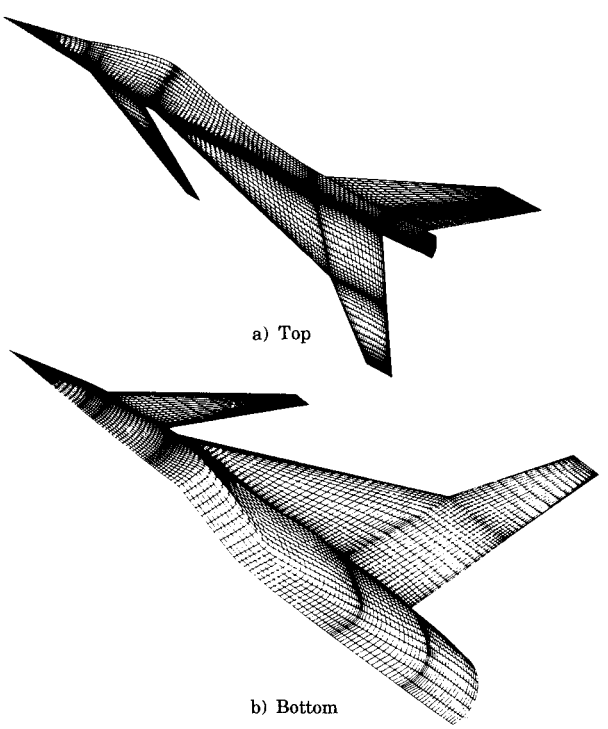

Fig. 1 Surface grid for a fighter aircraft.

Received Jan. 26, 1989; revision received Aug. 28, 1989.

*Graduate Research Assistant, Department of Mechanical Engineering and Mechanics. Student Member AIAA.

†Senior Research Engineer, ACD—Computer Applications Branch. Member AIAA.

‡Eminent Professor, Department of Mechanical Engineering and Mechanics. Associate Fellow AIAA.

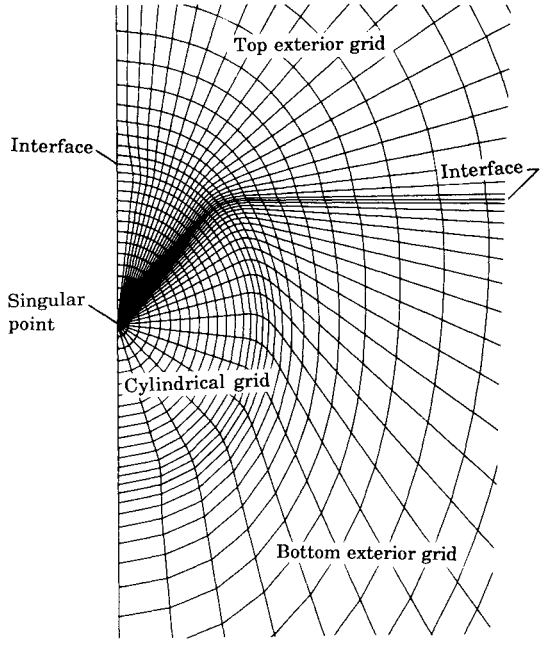

Fig. 2 Enlarged view of a cross cut of grids in the wake region.

called "multiple grid" or "zonal grid," subdivides the entire physical domain into several subdomains and subsequently several grid blocks. Subdomain grid-blocks are either patched together or partially overlapped. This approach has been investigated recently by several authors,[3-8] and it is clear that there are many strategies that can be pursued. When grid blocks are pathed together, several interface coupling strategies and treatments of boundary conditions are suggested in Refs. 9-13.

For the case where grid blocks can be patched together and there is grid continuity across interfaces, there are several existing grid-generation software systems available. For example, Thompson[14] has developed a composite (multiblock) numerical grid-generation program called EAGLE (Elgin Arbitrary Geometry Implicit Euler). This program is based on algebraic and elliptic grid-generation techniques and can be applied to a wide range of geometries.

In this study a multiple grid approach is used when several grids have naturally conservative interfaces, and an additional grid is adjoined with no continuity at the interfaces. The difficulty is the specification of an efficient mechanism to enforce conservation at the interfaces. An efficient technique called the "Ramshaw technique,"[15] which was originally devised to redistribute variables conservatively on Lagrangian grids, is applied. The application is Euler flow both around and through a fighter airplane configuration (see Fig. 1). An external grid and Euler flow with boundary conditions applied at the inlet are described in Ref. 16. Here, the previous external grid is extended into the wake region; an additional continuous grid block is computed for the region directly behind the fuselage, and an internal grid block is computed for a duct through the airplane. The duct grid interfaces with the external grid at an inlet and outlet where there is no grid alignment or continuity. The exterior and interior grid generation is based entirely on transfinite interpolation.[17] The Euler equations are solved with the internal and external grid blocks in the same manner, and the conservative interface procedure is applied at the interfaces between the internal and external blocks.

Grid Generation

The airplane configuration (see Fig. 1) for which supersonic flow is computed consists of a fuselage, canard, cranked delta wing, vertical fin, and inlet. A detailed discussion on this

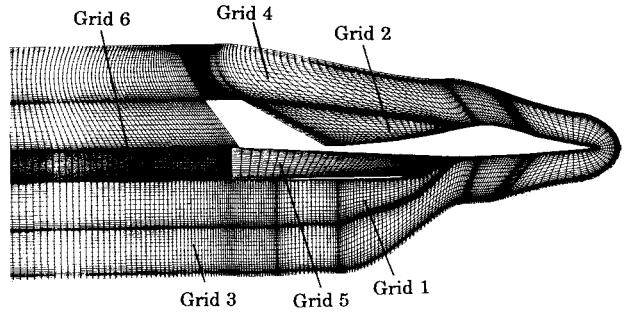

Fig. 3 Grid lines at the symmetry plane of the aircraft.

physical model is provided in Refs. 18 and 19. The first step in grid generation is the construction of a suitable surface grid that defines the geometry of the configuration. For the fighter configuration, this is achieved by a bicubic spline interpolation procedure.[20] Once a satisfactory surface grid is defined, the next task is to extend this grid into the flowfield. This is done by first establishing a grid topology which defines the block structure of the physical domain and then filling in the blocks with grid points. For the external grid, a dual-block topology and osculatory transfinite interpolation are used.[16]

In the present study, the flow domain is extended to include the wake region. A grid inside the inlet is also constructed to simulate internal flow simultaneously with the external flow. The interior grid is only required to patch with the exterior grid at the inlet intake and the exit plane. The extension of the exterior grid of Ref. 16 to include the wake region is achieved by extending the fuselage downstream and repeating the transfinite interpolation. However, the entire wake region is not covered by this extension. The void in the region directly behind the fuselage must also be covered with grid points. The region is filled with a cylindrical-type grid. This grid has a singularity line at the x axis of the physical coordinate system. Slope continuity at the interface between the cylindrical grid and the exterior grid is again obtained by osculatory transfinite interpolation. It is, however, not possible to have any kind of continuity at the interface between this grid and the interior grid since they are of completely different topologies.

The entire grid about the fighter configuration is, thus, divided into six subdomain grids. The surface grid for the configuration is shown in Fig. 1. The bottom and top grids are dual-block grids as described in Ref. 16. Figure 2 shows an enlarged view of cross-cut of grids in the wake region. The slope continuity at grid interfaces and the point of singularity are shown. Grid discontinuities at the interfaces between interior and exterior grids are clearly evident in Fig. 3 where grid lines are plotted at the symmetry plane. Figure 4 shows the connection of various computational subdomains. Here grids are numbered as indicated in the figure. The entire computational domain is composed of 493,641 grid points.

Governing Equations and Solution Procedure

For a fluid which has undergone no external forces, the Euler equations describing three-dimensional, unsteady, and compressible flow can be written as

$$\frac{\mathrm{d}}{\mathrm{d}t}\int_{\Omega} q\,\mathrm{d}x\,\mathrm{d}y\,\mathrm{d}z + \oint_{\partial\Omega} (n_x \cdot F + n_y \cdot G + n_z \cdot H)\,\mathrm{d}s = 0 \tag{1}$$

The quantities q, F, G, and H are defined in Refs. 13 and 19. The perfect gas equation of state is used to define the mean pressure P via the internal energy as

$$P = (\gamma - 1)\rho e \tag{2}$$

The Euler equation [Eq. (1)] is written in the integral form, and the solution procedure is based on a centered finite-volume scheme with explicit Runge-Kutta time-stepping.[21] This type of scheme was first used by Jameson et al.,[22] but the present scheme differs significantly from the original scheme mainly in the definition of the damping terms and the far-field boundary conditions.[19] It has been extensively tested in both two- and three-space dimensions and for both aerodynamic and turbomachinery applications.[2,23-25] Boundary conditions are mainly of three types: solid wall conditions, inflow/outflow (far-field) conditions, and interface conditions. The finite-volume discretization is described in the following subsection.

Spatial Finite-Volume Discretization

The simplest way to construct the centered finite-volume spatial discretization is to apply the integral formulation of the Euler equations [Eq. (1)] to each mesh cell of a given grid. The resulting semidiscrete scheme is written as

$$\mathrm{VOL}_{i,j,k}(\mathrm{d}/\mathrm{d}t)\, q_{i,j,k} + F_{i+\frac{1}{2},j,k} - F_{i-\frac{1}{2},j,k} + G_{i,j+\frac{1}{2},k} - G_{i,j-\frac{1}{2},k} + H_{i,j,k+\frac{1}{2}} - H_{i,j,k-\frac{1}{2}} = 0 \qquad (3)$$

In Eq. (3), $F_{i+\frac{1}{2},j,k}$, $G_{i,j+\frac{1}{2},k}$, and $H_{i,j,k+\frac{1}{2}}$ denote the approximate integrated flux of mass, momentum, and energy through the six cell walls of grid cell $[i, j, k]$. These integrated fluxes are computed by taking the average of the nonlinear flux functions evaluated at cell centers and multiplying these quantitites with the normal vector and surface area of the appropriate wall cell. Since the flux computations are symmetric, the resulting scheme is completely centered. It can be shown that the semidiscrete scheme [Eq. (3)] is conservative and second-order accurate on a smooth grid. The scheme is a cell concept rather than a grid-point concept. Therefore, it can be applied at mesh singularities without any special programming consideration. However, Eq. (3) is completely nondissipative due to the symmetric flux computations. In order to suppress aliasing and shock-induced oscillation, a mixture of second-difference and fourth-difference damping terms is added to Eq. (3). Here, the fourth-difference terms are global and linear, whereas the pressure-controlled, second-difference terms are nonlinear and are only activated around shocks.[16]

The boundary conditions are implemented according to the following requirements. At solid walls, only pressure is needed and is obtained by linear extrapolation from the two nearest cell centers. At inflow/outflow boundaries, an absorbing condition based on the theory of Engquist and Majda[26] is applied. At grid interfaces, the information outside the current subdomain grid is required for computing the integrated fluxes going through them. Since grid slopes are continuous at the interfaces of the exterior grids, fluxes at the cell faces are computed by taking the average of the flux functions evaluated at the center of these cells and at the center of the cells in the adjacent subdomain grid. The same procedure cannot be applied, however, at the interface between interior and exterior grids because grid lines are not continuous there. A method used to compute fluxes at these interfaces is described briefly in the following subsection.

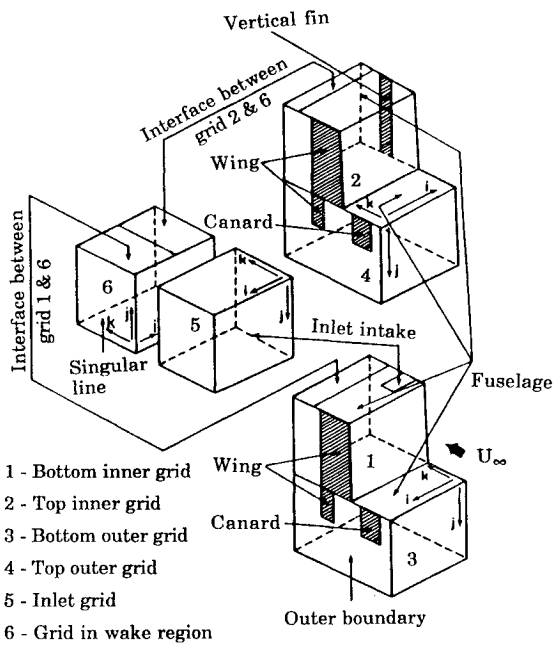

Fig. 4 Computational domains for the aircraft.

Interface Conditions

Consider an interface between two subdomain grids as shown in Fig. 5. The application of the finite-volume approach to the interface cells, denoted by $(i,j,NK-1)$, requires the integrated fluxes, $H^{(1)}_{i,j,NK-\frac{1}{2}} = (h^{(1)}_{i,j,NK-\frac{1}{2}})\,(A^{(1)}_{i,j,NK-\frac{1}{2}})$, where $A^{(1)}_{i,j,NK-\frac{1}{2}}$ are the cell surface areas at the interface. Recall from the preceding section that fluxes at the cell walls interior of the domain are computed by taking the average of the flux functions evaluated at cell centers, i.e., $h^{(1)}_{i,j,k+\frac{1}{2}} = \frac{1}{2}\,(h^{(1)}_{i,j,k} + h^{(1)}_{i,j,k+1})$. Thus, the evaluation of $h^{(1)}_{i,j,NK-\frac{1}{2}}$ requires the flux functions $h^{(1)}_{i,j,NK}$, which are located outside the domain (denoted as grid 1). They can be obtained by several ways. The simplest way is to extrapolate the quantities $h^{(1)}$ from the interior of the domain. Another way is to interpolate the quantities $h^{(2)}$ from the interior of the adjacent domain (grid 2 in Fig. 5). In this study, however, these interfaces are treated as the inflow/outflow boundaries and the theory of Engquist and Majda[26] is applied. Thus, $h^{(1)}_{i,j,NK-\frac{1}{2}}$ are obtained through the combination of the extrapolation and interpolation procedure according to whether the flow is supersonic or subsonic at the interfaces. Here, the incoming characteristic variables are fixed at the interpolated value rather than the freestream value as in the case of farfield boundaries. The details on the application of the theory are provided in Refs. 19 and 21.

To proceed with the computation onto the next subdomain grid (grid 2 in Fig. 5), the integrated fluxes $H^{(2)}_{i,j,-\frac{1}{2}}$ are required for grid cells $k = 1$. The value for $H^{(2)}_{i,j,-\frac{1}{2}}$ must be obtained from $H^{(1)}_{i,j,NK-\frac{1}{2}}$ conservatively to maintain the global conservation. To see how this can be done, consider a general interface as shown in Fig. 6. Here, solid lines represent grid lines at the interface of the subdomain grid (grid 1) with known quantities, i.e., $H^{(1)}_{i,j,NK-\frac{1}{2}}$. The dashed lines represent grid lines at the interface of the adjacent subdomain grid (grid 2) with unknown quantities, i.e., $H^{(2)}_{i,j,-\frac{1}{2}}$, to be obtained from $H^{(1)}_{i,j,NK-\frac{1}{2}}$ conservatively. In Fig. 6, $H^{(1)}_{i,j,NK-\frac{1}{2}}$ is written as $H^{(1)}_{i,j}$ and $H^{(2)}_{i,j,-\frac{1}{2}}$ as $H^{(2)}_{k\ell}$ to simplify the notation and avoid the confusion (since the subscript i,j appears in both quantities).

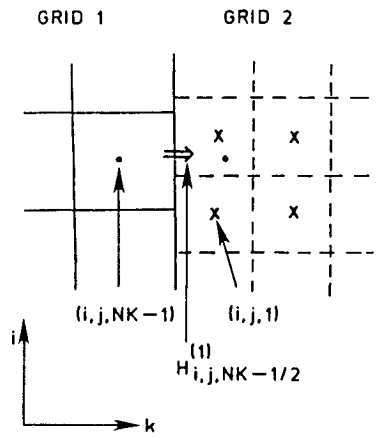

Fig. 5 Typical interface.

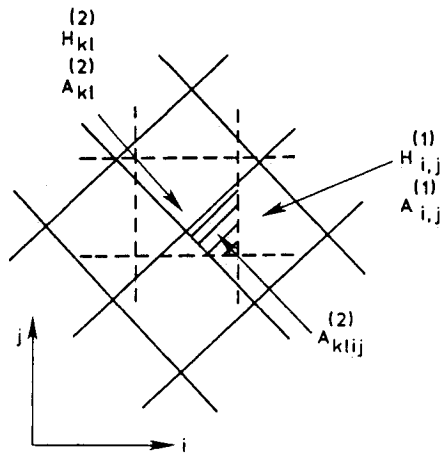

Fig. 6 Typical patched interface.

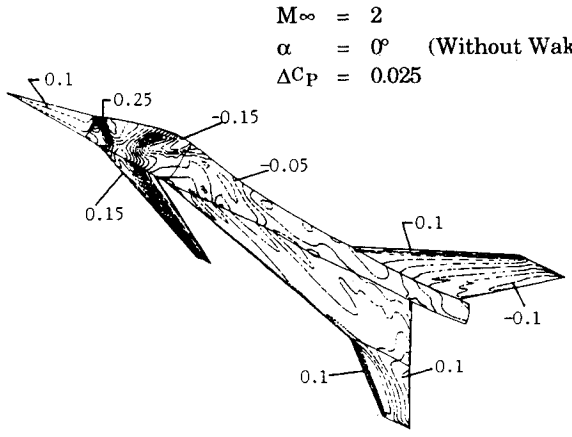

Fig. 7 Top surface C_p contours ($\alpha = 0$ deg, no wake).

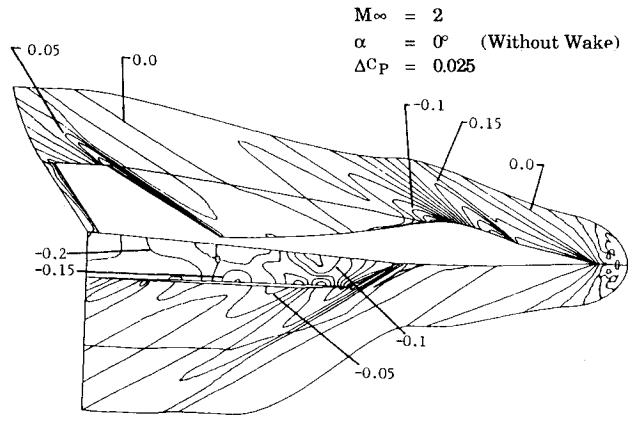

Fig. 8 Symmetry plane C_p contours ($\alpha = 0$ deg, no wake).

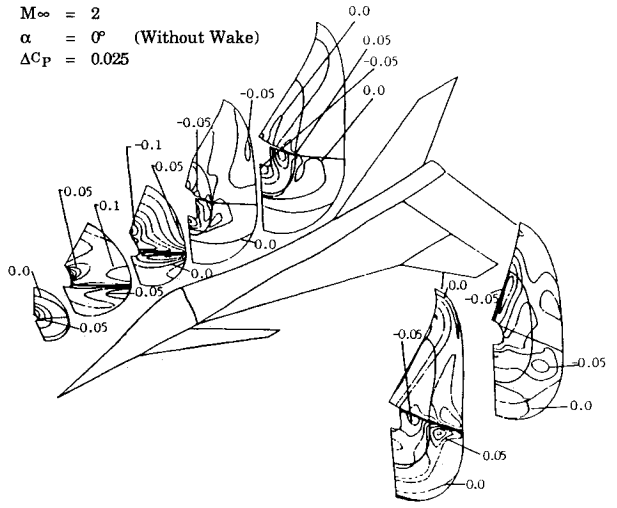

Fig. 9 Various cross cuts of C_p contours ($\alpha = 0$ deg, no wake).

The $A_{i,j}^{(1)}$ are the areas of the cell walls associated with $H_{ij}^{(1)}$, and $A_{k\ell}^{(2)}$ are areas associated with $H_{k\ell}^{(2)}$. Since $H_{i,j}^{(1)}$ are constant within each cell wall (i,j), $H_{k\ell}^{(2)}$ can be evaluated as (see Fig. 6)

$$H_{k\ell}^{(2)} = \sum_{n=1}^{P} H_{i,j}^{(1)} \cdot \frac{A_{k\ell ij}^{(2)}}{A_{i,j}^{(1)}} = \sum_{n=1}^{P} h_{i,j}^{(1)} \cdot A_{k\ell ij}^{(2)} \tag{4}$$

where $A_{k\ell ij}^{(2)}$ is the portion of the area $A_{k\ell}^{(2)}$ which is contained in the area $A_{i,j}^{(1)}$, and P is the number of the surface cells of grid 1, which is contained in the area $A_{k\ell}^{(2)}$. Since $h_{i,j}^{(1)}$ are known from the calculation in grid 1, the remaining task is to find the area $A_{k\ell ij}^{(2)}$ and the parameter P. This, however, is not trivial, and several methods have been suggested in the literature. This study follows the conservative rezoning method described by Dukowicz[27] and Ramshaw.[15] The method has been recently applied to solve the Euler flow over a Butler wing.[13] The method takes advantage of a formula to compute the area of a polygon in two dimensions as[28]

$$A_P = \tfrac{1}{2} \sum_{s} \epsilon_s^P (x_1^s y_2^s - x_2^s y_1^s) \tag{5}$$

where (x_1^s, y_1^s) and (x_2^s, y_2^s) are the endpoint coordinates of each line segments, the summation is over all of the sides of P, and ϵ_s^P is either $+1$ or -1 depending on whether P lies to the left or right of side s. It is very impractical to use Eq. (5) to compute the area of each polygon, i.e., $A_{k\ell ij}^{(2)}$, at a time since the number of sides of each polygon varies in general, and the parameter P in Eq. (4) also varies. However, it can be seen from Eq. (5) that the area A_P is only associated with the coordinate points (x_1^s, y_1^s) and (x_2^s, y_2^s); thus, it is possible to compute the area $A_{k\ell ij}^{(2)}$ by sweeping through grid lines, as suggested by Ramshaw. The details of this procedure can be found in Ref. 15.

Another method which can be used to compute the area $A_{k\ell ij}^{(2)}$ has been given by Hessenius and Rai.[29] The method makes use of the clipping algorithm as in computer graphic. Recently, Walters et al.[30] have applied the method to obtain solutions for flow over a hypersonic aircraft and forebodies.

Results and Discussion

The Euler solver described in the preceding section has been used to compute the flowfield about and through the Langley experimental fighter configuration (see Fig. 1 and Ref. 19). Steady-state solutions for supersonic flows have been obtained at a freestream Mach number of 2. Brief descriptions of steady-state solutions for flows at various angles of attack are presented. For flows without the wake region, the results are obtained for 0-, 3.79-, 7-, and 10-deg incidences. For the case of flow with the wake region, results are obtained for a 0-deg incidence. The computed flows are visualized in terms of pressure coefficient contours. A complete discussion of all available results is provided in Ref. 19. Some specific results are presented here in a somewhat logical sequence.

0-deg Angle of Attack (Without Wake)

Steady-state solutions for a freestream Mach number of 2 and 0-deg angle of attack are shown in Figs. 7-9. These figures show contours of the pressure coefficient on the surface of the airplane, on the symmetry plane, and on various cross cuts.

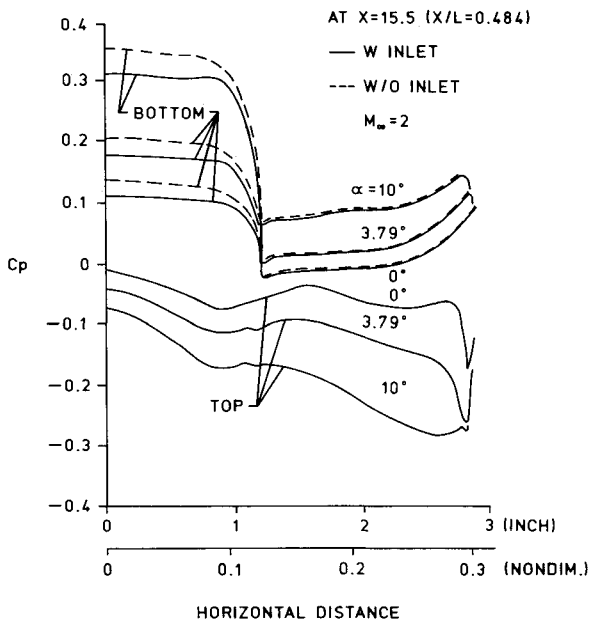

Fig. 10 Spanwise pressure distribution at the inlet intake (no wake).

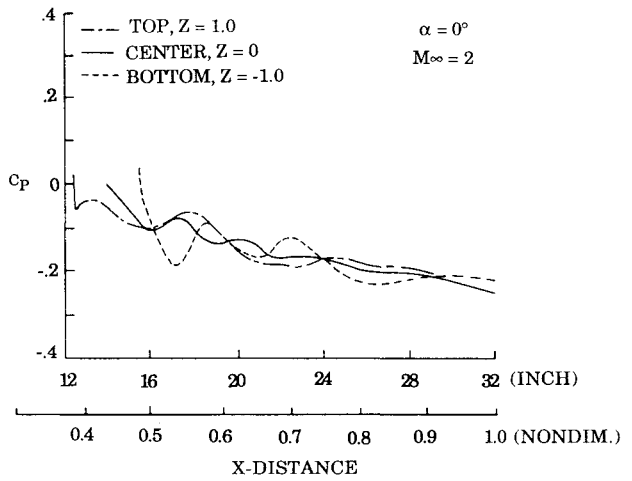

Fig. 11 Pressure distribution inside the inlet ($\alpha = 0$ deg, no wake).

The contours (along with the results presented in Ref. 19) display all the expected features of the flow with shocks emanating from the nose of the fuselage and from the leading edges of the lifting surfaces. The bulging (area ruling) of the fuselage behind the inlet gives rise to the higher pressure in the region on the fuselage and bottom wing surface just downstream of the inlet intake. Although the flow enters the inlet region in a smooth manner, there is considerable increase in pressure because of some chocking at the inlet intake.

The spanwise pressure distribution for $\alpha = 0$ deg, at a cross section which cuts through the inlet intake, is shown in Fig. 10 along with the results for $\alpha = 3.79$ and 10 deg. The solid line represents the solution from the present study, and the dashed line represents the result from the study of Ref. 16. In the figure, the horizontal distance is measured from the symmetry plane out to the wing tip. The distance is given as the real distance (in.) and the normalized distance. The normalized distance is based on the distance from the symmetry plane to the outer wing tip. The large pressure drops on the bottom surface occur at a distance of about 1.2 in. from the symmetry plane. This corresponds to the point where the wing starts on the bottom surface. The label "w/o inlet" in the figure simply

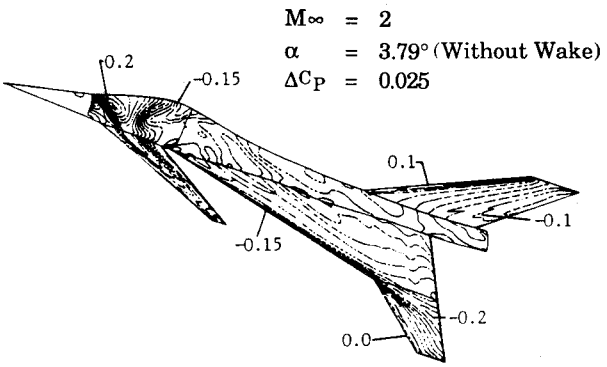

Fig. 12 Top surface C_p contours ($\alpha = 3.79$ deg, no wake).

means no simulation of flow inside the inlet but the inlet itself is still attached. The present results are seen to be lower than that of Ref. 16 at the inlet intake. This is because, in the present case, the flow is allowed to go through the inlet, whereas only the far-field condition (zero order extrapolation) is implemented in Ref. 16. The comparison demonstrates the influence of the flow inside the inlet to the external flow in the region near the inlet intake. It is expected that the flow in this region will change with the description of the inlet. No significant difference in results was noted for the top surface (see Ref. 19).

Variations in the pressure coefficient at the symmetry plane of the inlet are shown in Fig. 11 for three different locations (top, center, and bottom). The horizontal axis (x distance) in this figure is normalized with respect to the total length of the model (32 in. from the nose to the rear fuselage). The height of the inlet (z distance) is normalized based on its height from the centerline. The results show that the flow, in general, expands after it goes into the inlet. This is due to the inlet shape created by generation of the interior grid. However, the situation can be entirely different if another inlet shape is generated. The results also indicate that there exist shock waves, which bounce from the inlet walls. These shocks become weaker as the flow moves away from the inlet intake.

Different Angles of Attack (Without Wake)

Extensive results have been obtained for flows at 3.79-, 7-, and 10-deg angles of attack. Selected results are presented here, and results for other cases are provided in Ref. 19.

The pressure coefficient contours on the top surface of the configuration are shown in Fig. 12 for flow at a 3.79-deg angle of attack. It is seen that the high pressure region resulting from bulging of the fuselage moved forward on the bottom of the wing as compared to the case of the 0-deg angle of attack (see Fig. 7). It should be pointed out that this region moves forward with increasing angles of attack.[19] The comparison of the spanwise pressure distribution (see Fig. 10) indicates the same general trend as the case of a 0-deg angle of attack. This, again, demonstrates that the combination of implementation of the boundary conditions and simulation of the flow inside the inlet produces different results at the inlet intake. It is believed that simulation of the flow inside the inlet should produce a more realistic result. The variations in the pressure coefficient at the symmetry plane are shown in Fig. 13 along the top, center, and bottom of the inlet. Again, the expansion of the flow and the existence of shock waves which bounce from the walls can be seen clearly.

The pressure coefficient contours at the symmetry plane are provided in Reg. 19 for flow at a 7-deg angle of attack. A high pressure due to chocking is observed at the inlet intake. The low pressure in the inlet indicates that the flow expands while going through the inlet. This trend is similar to that observed in Figs. 11 and 13.

The results for a 10-deg angle of attack are shown in Figs. 10 and 14. The chocking of the flow at the inlet intake is evident from the contour plots of Fig. 14. The variation in pressure is higher in this case in comparison to the previous cases of lower angles of attack. A comparison of results presented in Fig. 10 also indicates the influence of the flow inside the inlet on the external flow in the region near the inlet intake. In obtaining these results, numerical oscillations were noted near the leading edge of the inner wing. Such oscillations were also observed in the study of Ref. 16. Further investigation indicates that the oscillation only occurs at a certain region, i.e., a region just inside the top leading edge of the 70-deg swept portion of the wing. Elsewhere, the residuals are well below the convergence criterion. Further discussions on this is available in Refs. 16 and 19.

Variations in the pressure coefficient along the centerline of the symmetry plane from the freestream to the exit plane of the inlet are illustrated in Fig. 15 for different angles of attack. The results indicate a similar pattern for each angle of attack. Shock waves generated at the nose of the aircraft and near the inlet intake (due to chocking) are clearly visible. The expansion of flows inside the inlet and interaction of shock waves from the walls are clearly evident. It is seen that pressure increases with increasing the angle of attack.

0-deg Angle of Attack (with Wake)

The pressure coefficient contours on the top and bottom surfaces of the fuselage, canard, and wing are provided in Ref. 19. These contours are similar to those obtained for the case without the wake except near the end of the fuselage. A lower pressure (as compared to flows without the wake region) is observed in the region of the rear fuselage due to simulation of the flow in the wake region. The influence of the flow in the wake region is clearly seen in Fig. 16. The spanwise pressure distribution from three different solutions are compared at 98% of the configuration ($x = 31.5$ in.). The solid line represents the case of flow with the inlet and wake region. The other two curves represent the cases of flow without the wake region. At this particular location, the two solutions without the wake region agree very well. However, they indicate a higher pressure than that obtained for the flow with the wake region. This is because the outflow boundary condition has to be given right at the boundary of the domain (at the end of the fuselage for the case without the wake region). This condition arises because the computational domain has to be closed for practical reasons. The farther this boundary moves away from the configuration, the closer the computational model is to the real situation. A primary reason previous studies do not extend the domain beyond the end of the fuselage is due to the difficulty in generating a grid in that region. Moreover, the condition at the exit plane of the inlet is unknown. The jet afterbody interaction can also influence the flow in the region near the fuselage. Indeed, it is the ultimate goal of this study to overcome such difficulties and be able to model the flow as close to the real situation as possible. The pressure coefficient contours at the plane of symmetry (see Fig. 17) indicate a strong interaction between the jet and afterbody flows. Contours in the front

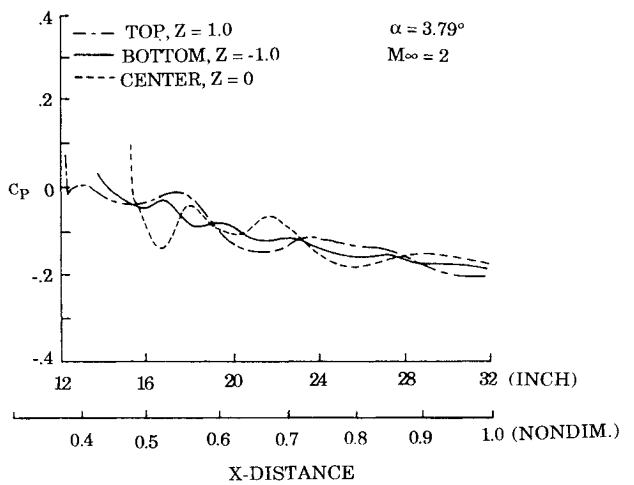

Fig. 13 Pressure distribution inside the inlet ($\alpha = 3.79$ deg, no wake).

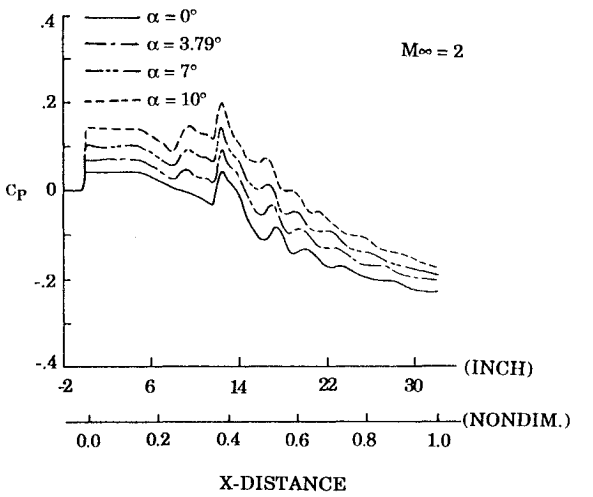

Fig. 15 Pressure distribution from freestream to exit plane of the inlet for various angles of attack.

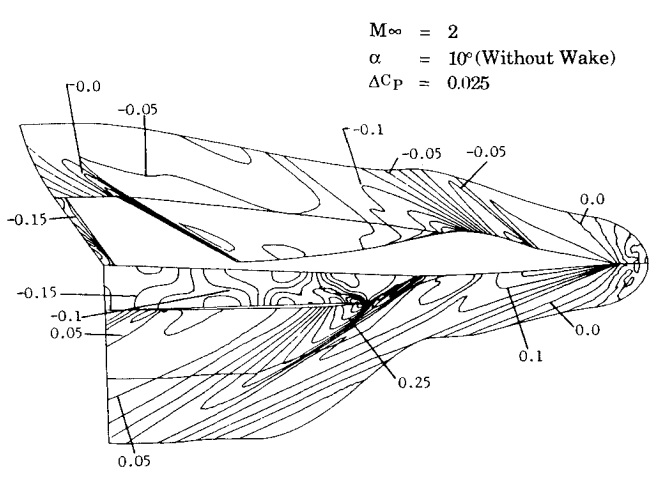

Fig. 14 Symmetry plane C_p contours ($\alpha = 10$ deg, no wake).

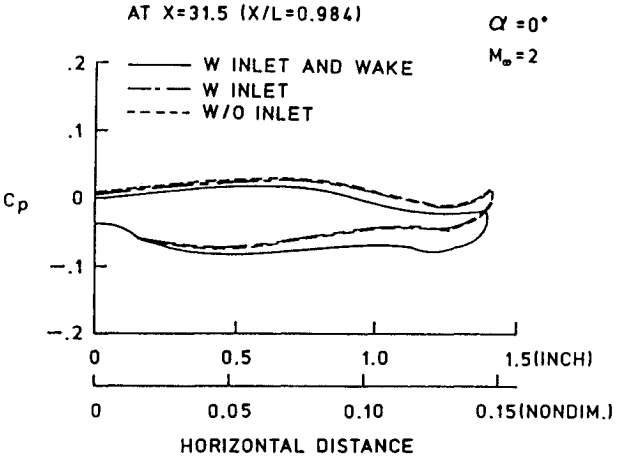

Fig. 16 Spanwise pressure distribution near the end of the fuselage ($\alpha = 0$ deg, with wake).

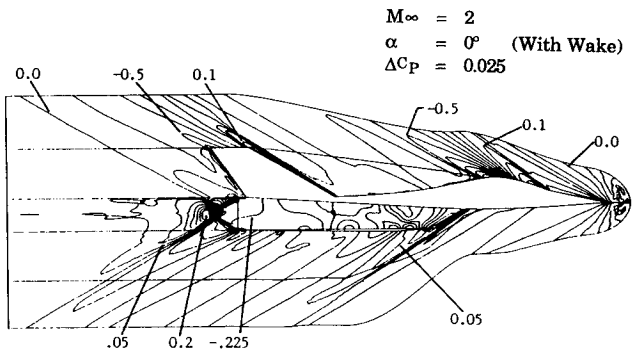

Fig. 17 Symmetry plane C_p contours ($\alpha = 0$ deg, with wake).

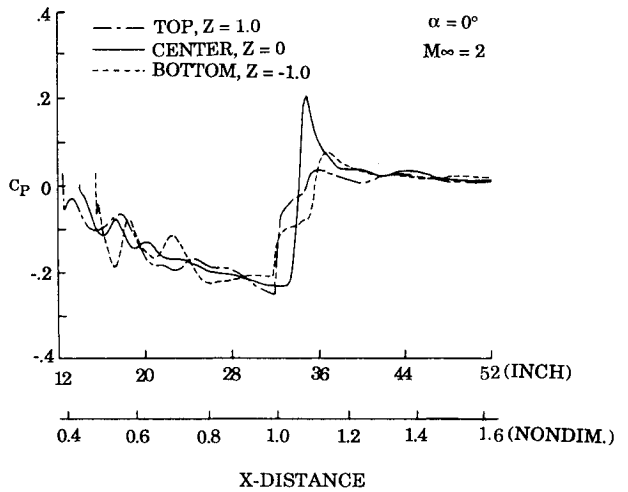

Fig. 18 Pressure distribution from the inlet intake to end of the wake region.

of the configuration display the same features as seen in the case of flow without the wake region. In the wake region, the flow coming out of the exit plane of the inlet (jet) has a lower pressure but higher velocity than the external flow around the airplane (afterbody flow). As a result of this interaction, the internal flow gets compressed and external flow is expanded. The shock waves emanating from the rear fuselage meet farther downstream and reflect off each other. Also, the flows are not symmetric about the middle of the jet because the top of the configuration includes the wings and vertical fin. It should be mentioned that accuracies cannot be claimed for solutions in the wake region. Realistically, flow in this region becomes turbulent and the Navier-Stokes equations with an appropriate turbulent modeling must be used. This study, however, has taken a step toward that goal since it is now possible to generate grids to cover both internal and external regions.

The pressure coefficient variations at the plane of symmetry are illustrated in Fig. 18 for three different locations. The plots start at the inlet intake and end at the end of the domain in the wake region. Inside the inlet, i.e., $12 \le x \le 32$ (or $0.4 \le X/L \le 1.0$), the results are the same as those of the case without the grid in the wake region (see Fig. 11). The flow expands and shock waves bounce from the inlet walls. At the exit plane of the inlet, the internal flow starts interacting with the external flow from the top and bottom of the inlet. The jet coming out of the center of the inlet, however, does not interact with the afterbody flow until a little farther distance downstream. These are indicated by the jumps in pressures. The flow enters the inlet supersonically and is accelerated as it goes through the inlet. The flow exits the inlet supersonically with a rather high velocity. This velocity is much higher than that of the afterbody flow. Thus, there exist oblique shock waves and vortical flow in this region. The shock waves meet farther downstream and produce a high-pressure region behind them. Thus, the pressure jump at the center line occurs a little farther downstream, and its magnitude is relatively higher. It should be noted that the flow in the wake region displays a similar feature as the classical free jet exhausting from a supersonic nozzle.

Concluding Remarks

The objective of this study has been to demonstrate the use of the multiple grids approach (without grid continuities at the interfaces of various grids) to obtain solutions of physical problems where the use of a single grid may not be feasible. Specific attention is directed to obtain the steady-state solutions of the Euler equations for flows over a complex fighter-aircraft configuration. The solutions are obtained for a freestream Mach number of 2 and for 0-, 3.79-, 7-, and 10-deg angles of attack for the case of internal/external flow interaction without the wake region. The extension of the domain to include the flow in the wake region is also investigated. The results demonstrate that it is possible to construct grids about complex configurations by using multiple grids with or without continuous interfacing. The method is capable of computing internal and external flows simultaneously.

It is demonstrated that modeling of the flow inside the engine inlet and in the wake region influences the flow around the airplane. It should be noted that the exact description of the engine inlet is not available. It is modeled by applying the transfinite interpolation procedure to "fill" the region between the inlet intake and the exit plane. It is expected that the inlet description will influence the external flow at least in the region close to it.

Acknowledgments

The authors would like to express their appreciation to Michael R. Wiese of the Computer Sciences Corporation for the discussion of plots obtained from Ref. 16. This work was supported partially by the NASA Langley Research Center through Grant NCC1-68.

References

[1]Jameson, A., and Baker, T. J., "Multigrid Solution of the Euler Equations for Aircraft Configurations," AIAA Paper 84-0093, Jan. 1984.

[2]Eriksson, L.-E., and Rizzi, A. W., "Computation of Vortex Flow Around a Canard/Delta Combination," *Journal of Aircraft*, Vol. 21, No. 11, Nov. 1984.

[3]Rai, M. M., "A Conservative Treatment of Zonal Boundaries for Euler Equation Calculations," AIAA Paper 84-0164, Jan. 1984; also, "A Relaxation Approach to Patched-Grid Calculations with the Euler Equations," *Journal of* Computational Physics, Vol. 66, No. 1, Sept. 1986, pp. 99-131.

[4]Karman, S. L., Jr., Steinbrenner, J. P., and Kisielewski, K. M., "Analysis of the F-16 Flow Field by a Block Grid Euler Approach," 58th Meeting of the Fluid Dynamics Panel Symposium on Application of Computational Fluid Dynamics in Aeronautics, Aix-En-Provence, France, April 1986.

[5]Weatherill, N. C., and Forsey, C. R., "Grid Generation and Flow Calculations for Complex Aircraft Geometries Using a Multi-Block Scheme," AIAA Paper 84-1665, June 1984.

[6]Berger, M. J., and Jameson, A., "Automatic Adaptive Grid Refinement for the Euler Equations," *AIAA Journal*, Vol. 23, April 1985, pp. 561-568.

[7]Eriksson, L.-E., "Euler Solutions on 0-0 Grids Around Wings Using Local Refinement," *Proceedings of the 6th GAMM Conference on Numerical Methods in Fluid Mechanics*, edited by D. Rues and W. Kodulla, Vieweg Verlag, Göttigen, Sept. 1985.

[8]Benek, J. A., Buning, P. G., and Steger, J. L., "A 3-D Chimera Grid Embedding Technique," AIAA Paper 85-1523, July 1985.

[9]Berger, M. J., "On Conservation at Grid Interfaces," Institute for Computer Applications in Science and Engineering, NASA Langley Research Center, Hampton, VA, ICASE Rept. 84-43, Sept. 1984;

also, *SIAM Journal of Numerical Analysis*, Vol. 24, No. 5, Oct. 1987, pp. 967–984.

[10]Doutherty, F. C., "Development of a Chimera Grid Scheme with Applications to Unsteady Problems," Ph.D. Thesis, Dept. of Aeronautics and Astronautics, Stanford University, Palo Alto, CA, May 1985.

[11]Miki, K., and Takagi, T., "A Domain Decomposition and Overlapping Method for the Generation of Three-Dimensional Boundary-Fitted Coordinate Systems," *Journal of Computational Physics*, Vol. 53, No. 2, Feb. 1984, pp. 319–330.

[12]Rubbert, P. E., and Lee, K. D., "Patched Coordinate Systems," *Numerical Grid Generation*, edited by J. F. Thompson, North-Holland, New York, 1982, pp. 235–252.

[13]Kathong, M., Smith, R. E., and Tiwari, S. N., "A Conservative Approach for Flow Field Calculation on Multiple Grids," AIAA Paper 88-0224, Jan. 1988.

[14]Thompson, J. F., "A Composite Grid Generation Code for General 3D Regions—the EAGLE Code," *AIAA Journal*, Vol. 26, No. 3, March 1988, pp. 271–272.

[15]Ramshaw, J. D., "Conservative Rezoning Algorithm for Generalized Two-Dimensional Meshes," *Journal of Computational Physics*, Vol. 59, June 1985, pp. 193–199.

[16]Eriksson, L.-E., Smith, R. E., Wiese, M. R., and Farr, N., "Grid Generation and Inviscid Flow Computation About Cranked-Winged Airplane Geometries," AIAA Paper 87-1125, June 1987; also, *Journal of Aircraft*, Vol. 25, No. 9, Sept. 1988, pp. 820–826.

[17]Eriksson, L.-E., "Practical Three-Dimensional Mesh Generation Using Transfinite Interpolation," *SIAM Journal on Scientific and Statistical Computing*, Vol. 6, No. 3, July 1985, pp. 712–741.

[18]Hom, K. W., and Ticatch, L. A., "Investigation of an Advanced Supersonic Fighter Concept Including Effects of Horizontal Tail and Canard Control Surfaces Over a Mach Number Range From 1.6 to 2.5," NASA-TP 2526, May 1986.

[19]Kathong, M., and Tiwari, S. N., "Application of Advanced Grid Generation Techniques for Flow Field Computations About Complex Configurations," NASA-CR-183049, NAS 1.26:183049, July 1988; also, Ph.D. Dissertation by M. Kathong, Old Dominion University, Norfolk, VA, Aug. 1988.

[20]Smith, R. E., "Algebraic Grid Generation About Wing-Fuselage Bodies," 15th Congress of the International Council of the Aeronautical Sciences, London, UK, Sept. 1986.

[21]Rizzi, A. W., and Eriksson, L.-E., "Computational of Flow Around Wings Based on the Euler Equations," *Journal of Fluid Mechanics*, Vol. 148, March 1984, pp. 45–71.

[22]Jameson, A., Schmidt, W., and Turkel, E., "Numerical Solutions of the Euler Equations by Finite Volume Methods Using Runge-Kutta Time-Stepping Schemes," AIAA Paper 81-1259, June 1981.

[23]Rizzi, A., and Eriksson, L.-E., "Computation of Inviscid Incompressible Flow with Rotation," *Journal of Fluid Mechanics*, Vol. 153, Oct. 1985, pp. 275-312.

[24]Eriksson, L.-E., "Simulation of Inviscid Flow Around Airfoils and Cascades Based on the Euler Equations," The Aeronautical Research Institute of Sweden, Stockholm, FFA TN-1985-20, 1985.

[25]Eriksson, L.-E., "Simulation Transonic Flow in Radial Compressors," *Computer Methods in Applied Mechanics and Engineering*, Vol. 64, Nos. 1-3, Oct. 1987, pp. 95–111.

[26]Engquist, B., and Majda, A., "Absorbing Boundary Conditions for the Numerical Simulation of Waves," *Mathematics of Computation*, Vol. 31, July 1977, pp. 629–651.

[27]Dukowicz, J. K., "Conservative Rezoning (Remapping) for General Quadrilateral Meshes," *Journal of Computational Physics*, Vol. 54, June 1984, pp. 411–424.

[28]Rektorys, K. (ed.), *Survey of Applicable Mathematics*, MIT Press, Cambridge, MA, 1969, p. 207.

[29]Hessenius, K. A., and Rai, M. M., "Three-Dimensional, Conservative, Euler Computations Using Patched Grid Systems and Explicit Methods," AIAA Paper 86-1081, May 1986.

[30]Walters, R. W., Reu, T., McGrory, W. D., Thomas, J. L., and Richardson, P. F., "A Longitudinally-Patched Grid Approach with Applications to High Speed Flows," AIAA Paper 88-0715, Jan. 1988.